Available online at www.sciencedirect.com
ScienceDirect
Journal of the European Ceramic Society 27 (2007) 2009–2016
www.elsevier.com/locate/jeurceramsoc

Structural and electrical properties of MgO-doped $Mn_{1.4}Ni_{1.2}Co_{0.4-x}Mg_xO_4$ ($0 \leq x \leq 0.25$) NTC thermistors

K. Park [a,*], S.J. Kim [a], J.-G. Kim [b], S. Nahm [c]

[a] *Faculty of Nanotechnology and Advanced Materials Engineering, Sejong University, Seoul 143-747, Republic of Korea*
[b] *Inorganic Chemistry Examination Division, Korean Intellectual Property Office, Daejeon 302-701, Republic of Korea*
[c] *Department of Materials Science and Engineering, Korea University, Seoul 136-701, Republic of Korea*

Received 5 February 2006; received in revised form 13 July 2006; accepted 21 July 2006
Available online 11 September 2006

Abstract

We have prepared polycrystalline $Mn_{1.4}Ni_{1.2}Co_{0.4-x}Mg_xO_4$ ($0 \leq x \leq 0.25$) samples using a solid-state reaction process and investigated the MgO doping effect on the microstructure and the electrical properties. It was found that, as the amount of Mg content in the $Mn_{1.4}Ni_{1.2}Co_{0.4-x}Mg_xO_4$ samples increased, both the grain size and density decreased. The as-sintered $Mn_{1.4}Ni_{1.2}Co_{0.4-x}Mg_xO_4$ samples contained Mn- and Ni-rich phases with cubic spinel structure. The MgO-doped $Mn_{1.4}Ni_{1.2}Co_{0.4-x}Mg_xO_4$ negative temperature coefficient (NTC) thermistors provided various electrical properties, depending on Mg content. The electrical resistivity, $B_{25/85}$ constant, and activation energy of the $Mn_{1.4}Ni_{1.2}Co_{0.4-x}Mg_xO_4$ NTC thermistors increased with increasing Mg content. The values of ρ_{25}, $B_{25/85}$ constant, and activation energy of the NTC thermistors were 11,185–20,016 Ω cm, 3635–4032 K, and 0.313–0.348 eV, respectively.

Keywords: NTC thermistor; Electrical conductivity; Electrical properties; Transition metal oxides; Sintering

1. Introduction

Transition metal manganites $Mn_{3-x}M_xO_4$ (M = Ni, Cu, Fe, Co, etc.) are technologically important materials used as negative temperature coefficient (NTC) thermistor materials owing to their interesting electrical properties.[1] Their electrical resistivity ρ varies exponentially with temperature T by the well known Arrhenius equation $\rho = \rho_o \exp(B/T)$,[1] where ρ_o is the resistivity of the material at infinite temperature and B is the B constant which is a measure of the sensitivity of the device over a given temperature. Here, the B constant has the dimensions of the absolute temperature and is given by the equation $B = E_a/k_B$, where E_a is the activation energy for electrical conduction and k_B is the Boltzmann constant. The activation energy is primarily the energy for the hopping process from a cation M^{n+} to $M^{(n+1)+}$ on the octahedral sites and, hence, for the mobility of the cations.[2–6]

The B constant can be calculated by Eq. (1):[1]

$$B = \frac{\ln \rho_1 - \ln \rho_2}{1/T_1 - 1/T_2} \quad (1)$$

where ρ_1 and ρ_2 are the resistivities measured at temperatures T_1 and T_2, respectively.

The oxides typically exhibit the spinel-type crystal structure with the general formula $A[B_2]O_4$.[6–9] In this structure, a cubic close packed array of oxygen ions allows two types of lattice sites available for the cations with tetrahedral site, the A-site, and the octahedral site, the B-site. In general, the lattice site occupation can change, i.e., between the extremes of a so-called normal spinel, $A[B_2]O_4$ and an inverse one, $B[AB]O_4$. NTC thermistors are widely used in a variety of industrial areas such as automotive, cellular phone, telecommunication, and aerospace, e.g., elements for the suppression of in-rush current, for temperature measurements and control, and for compensation for other circuit elements.[10–12] The selection of a given metal oxide material for the applications of NTC thermistors is mainly determined by the required resistivity and the $B_{25/85}$ constant, i.e., the thermal sensitivity.

* Corresponding author. Tel.: +82 2 34083777; fax: +82 2 34083664.
E-mail address: kspark@sejong.ac.kr (K. Park).

0955-2219/$ – see front matter © 2006 Elsevier Ltd. All rights reserved.
doi:10.1016/j.jeurceramsoc.2006.07.002

In general, the electrical properties depend on the composition, which influences the distribution of cations in the spinel structure.[13–17] In the present study, we studied the microstructure and electrical properties of the $Mn_{1.4}Ni_{1.2}Co_{0.4-x}Mg_xO_4$ NTC thermistors fabricated by the solid-state reaction method, especially with regard to the partial substitution of Mg for Co in $Mn_{1.4}Ni_{1.2}Co_{0.4}O_4$.

2. Experimental

High-purity Mn_3O_4, NiO, Co_3O_4, and MgO powders were weighed in appropriate proportions to fabricate $Mn_{1.4}Ni_{1.2}Co_{0.4-x}Mg_xO_4$ ($x = 0$, 0.05, 0.10, 0.15, 0.20, and 0.25). The mixture of weighed powders and distilled water was milled for 6 h using a planetary mill (FRITSCH pulverisette 6) and a ZrO_2 ball as grinding media. The resulting slurries were dried at 80 °C in an oven for 24 h. The dried powders were then ground carefully in mortar and passed through a 250-mesh sieve. Thermal analysis of the oxide mixtures was carried out using a differential thermal/thermogravimetric analysis (DT/TGA) (SCINCO Co. STA S-1500) in the temperature range of 0–1200 °C at a heating rate of 10 °C min^{-1} in air. The granulated powders were calcined in a mullite crucible at 950 °C for 2 h. Distilled water and polyvinyl alcohol (PVA) were then added into the calcined powders, and the mixtures were further milled for 3 h using a planetary mill (FRITSCH pulverisette 6)

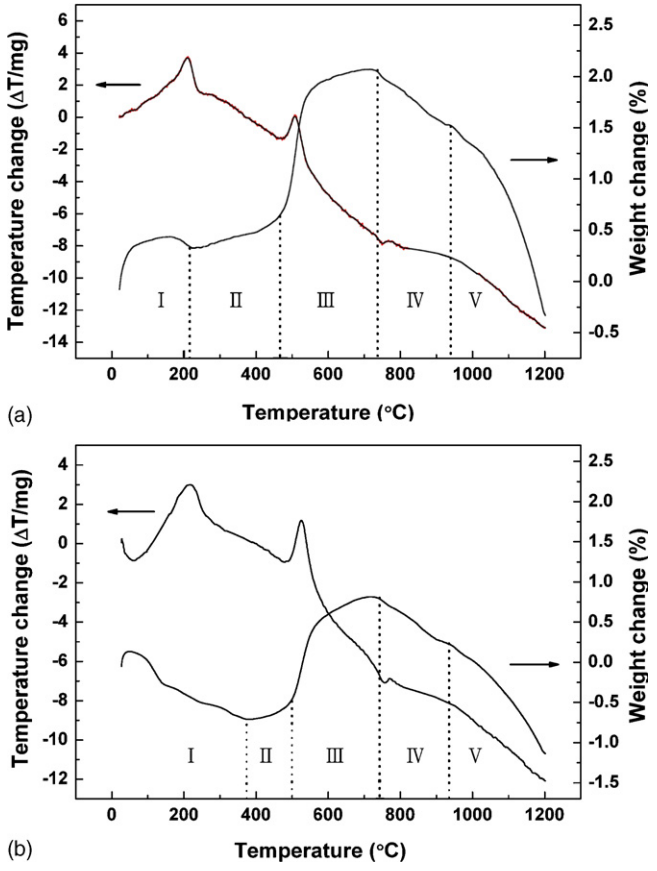

Fig. 1. Results of the DTA and TGA measurements for a mixture of the oxide powders of: (a) $Mn_{1.4}Ni_{1.2}Co_{0.4}O_4$ and (b) $Mn_{1.4}Ni_{1.2}Co_{0.15}Mg_{0.25}O_4$ samples.

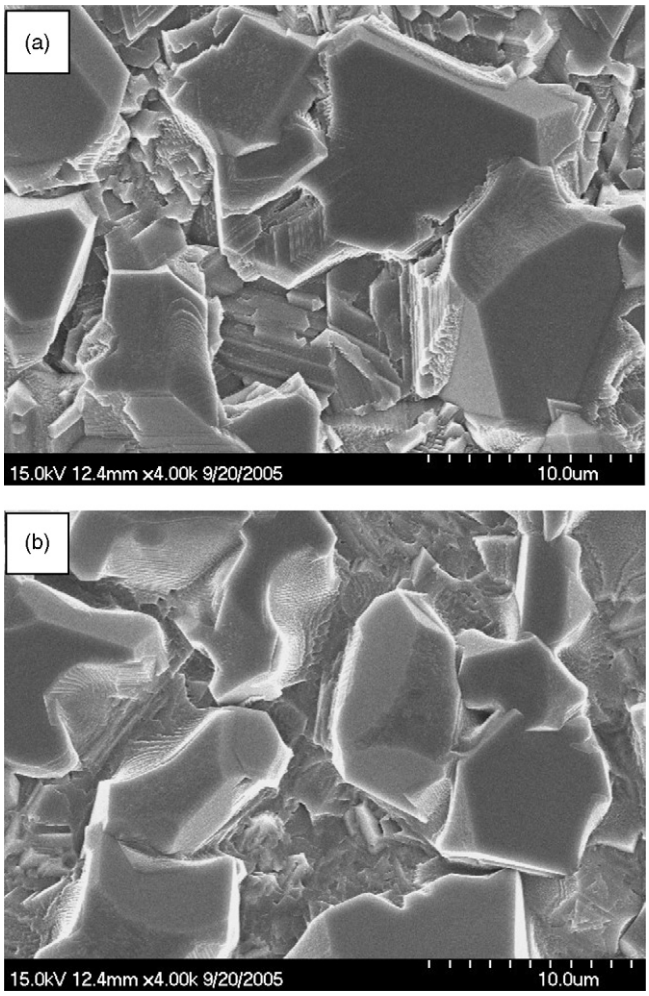

Fig. 2. SEM images obtained from the surface of: (a) $Mn_{1.4}Ni_{1.2}Co_{0.4}O_4$ and (b) $Mn_{1.4}Ni_{1.2}Co_{0.2}Mg_{0.2}O_4$ samples sintered at 1260 °C.

and ZrO_2 as grinding media. The resulting slurries were dried at 80 °C in an oven for 24 h. The dried powders were then ground carefully in mortar and passed through a 250-mesh sieve. Subsequently, the mixture of powders was pressed using a hand press at a pressure of 49 MPa to prepare pellets of 1 mm-thick and 8-mm in diameter. The green compacts were heated at 950–1260 °C for 3 h in air, and then furnace cooled.

The crystalline structure of the as-sintered $Mn_{1.4}Ni_{1.2}Co_{0.4-x}Mg_xO_4$ samples was analyzed with X-ray diffraction (XRD) (Rigaku DMAX 2500) using Cu Kα radiation at 40 kV and 25 mA. The microstructure of the samples was investigated by a scanning electron microscope (SEM) (Hitachi S4200). In order to identify the distribution of constituent elements in the as-sintered ceramics, secondary electron images (SEI) and elemental maps were investigated using an electron probe microanalysis (EPMA). The Ag paste with thicknesses of ~15 μm was spread on opposite-side surfaces of the sintered samples using a screen printer. After the paste was dried at room temperature, the samples were heated at 850 °C for 10 min. Ten samples of each composition for measuring electrical resistance were prepared. The samples were held with a holder in a bath of silicone oil, and their temperatures were measured with a digital ther-

mometer. The electrical resistance was measured with a digital multimeter (Fluke 45) from 25 up to 115 °C in steps of 10 °C.

3. Results and discussion

Fig. 1(a and b) shows the results of the DTA and TGA measurements for a mixture of the oxide powders of $Mn_{1.4}Ni_{1.2}Co_{0.4}O_4$ and $Mn_{1.4}Ni_{1.2}Co_{0.15}Mg_{0.25}O_4$ samples, respectively. In low temperature region, region I, it is seen that there are exothermic peaks at 211 and 229 °C for the $Mn_{1.4}Ni_{1.2}Co_{0.4}O_4$ and $Mn_{1.4}Ni_{1.2}Co_{0.15}Mg_{0.25}O_4$ samples, respectively, accompanied with the weight loss. This is due to the removal of absorbed water and organic volatiles present in the samples.[18] In addition, we can find the weight change for the two samples due to several oxido-reduction phenomena.[19,20] A slight weight gain in region II is closely associated with the oxidation of Mn^{3+} cations on octahedral sites.[20] When the temperature is further increased (region III), a drastic weight increase occurred because of the oxidation of the tetrahedral Mn^{2+}. This observation is supported by DTA studies, i.e., the presence of the exothermic peaks in the DTA curves located at around 507 and 525 °C for $Mn_{1.4}Ni_{1.2}Co_{0.4}O_4$ and $Mn_{1.4}Ni_{1.2}Co_{0.15}Mg_{0.25}O_4$ samples, respectively. For higher temperatures than region III, region IV, a gradual weight loss originates from the reduction of Mn^{4+} to Mn^{3+} ions. Finally, for the highest temperature region, region V, we can find a significant weight loss of the powders, which is attributed to the reduction of Mn^{3+} ions and the loss of excess oxygen, and the stoichiometry of the sample is progressively restored.[20]

Table 1
Lattice parameters of the $Mn_{1.4}Ni_{1.2}Co_{0.4-x}Mg_xO_4$ samples sintered at 1260 °C

Sample		Lattice parameter (Å)
$Mn_{1.4}Ni_{1.2}Co_{0.4}O_4$	Mn-rich region	8.339
	Ni-rich region	8.269
$Mn_{1.4}Ni_{1.2}Co_{0.35}Mg_{0.05}O_4$	Mn-rich region	8.328
	Ni-rich region	8.263
$Mn_{1.4}Ni_{1.2}Co_{0.3}Mg_{0.1}O_4$	Mn-rich region	8.321
	Ni-rich region	8.258
$Mn_{1.4}Ni_{1.2}Co_{0.25}Mg_{0.15}O_4$	Mn-rich region	8.314
	Ni-rich region	8.255
$Mn_{1.4}Ni_{1.2}Co_{0.2}Mg_{0.2}O_4$	Mn-rich region	8.303
	Ni-rich region	8.219
$Mn_{1.4}Ni_{1.2}Co_{0.15}Mg_{0.25}O_4$	Mn-rich region	8.298
	Ni-rich region	8.198

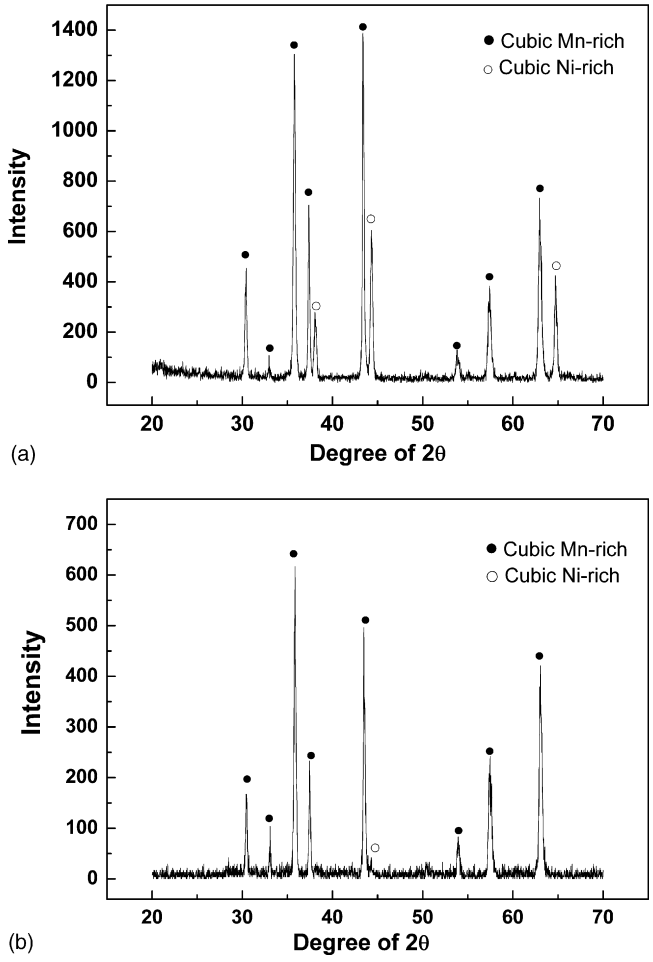

Fig. 3. XRD patterns of: (a) $Mn_{1.4}Ni_{1.2}Co_{0.4}O_4$ and (b) $Mn_{1.4}Ni_{1.2}Co_{0.2}Mg_{0.2}O_4$ samples sintered at 1260 °C.

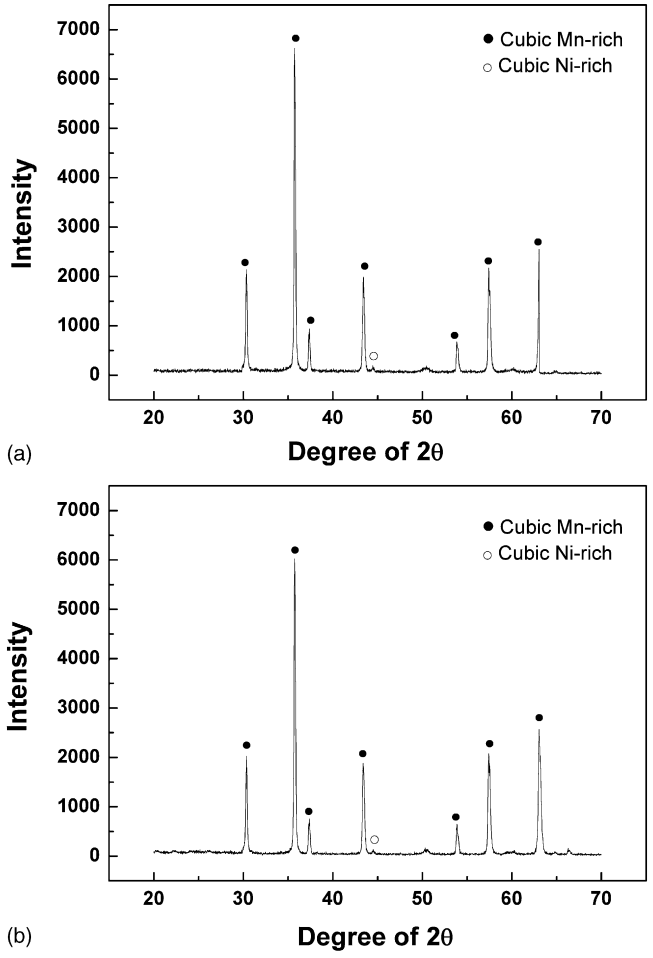

Fig. 4. XRD patterns of: (a) $Mn_{1.4}Ni_{1.2}Co_{0.4}O_4$ and (b) $Mn_{1.4}Ni_{1.2}Co_{0.2}Mg_{0.2}O_4$ samples sintered at 950 °C.

The SEM images obtained from the surface of the $Mn_{1.4}Ni_{1.2}Co_{0.4}O_4$ and $Mn_{1.4}Ni_{1.2}Co_{0.2}Mg_{0.2}O_4$ samples sintered at 1260 °C are shown in Fig. 2(a and b), respectively. The mean grain sizes of the as-sintered $Mn_{1.4}Ni_{1.2}Co_{0.4}O_4$ and $Mn_{1.4}Ni_{1.2}Co_{0.2}Mg_{0.2}O_4$ samples were 4.9 and 3.7 μm, respectively. This represents that the substituted Mg retarded the grain growth during sintering. This is mainly attributed to the fact that the interaction forces between the added MgO and grain boundaries exert a dragging effect on the migration of the boundaries, retarding the grain growth. A similar behavior was reported for MgO-doped Al_2O_3.[21] The grain growth rate of MgO-doped Al_2O_3 was much lower than that of undoped Al_2O_3. It was also observed that the $Mn_{1.4}Ni_{1.2}Co_{0.4-x}Mg_xO_4$ ($0 \leq x \leq 0.25$) samples were highly dense. For example, the densities of $Mn_{1.4}Ni_{1.2}Co_{0.4}O_4$ and $Mn_{1.4}Ni_{1.2}Co_{0.2}Mg_{0.2}O_4$ samples were 99 and 96% of the theoretical density, respectively. A dense microstructure is necessary to obtain a good reproducibility of the electrical characteristics of the ceramics.

The XRD patterns of the $Mn_{1.4}Ni_{1.2}Co_{0.4}O_4$ and $Mn_{1.4}Ni_{1.2}Co_{0.2}Mg_{0.2}O_4$ samples sintered at 1260 °C are shown in Fig. 3(a and b), respectively. The sintered samples were composed of the Mn- and Ni-rich phases with the cubic spinel structure. The two separated phases originate from the decomposition of the cubic spinel $Mn_{1.4}Ni_{1.2}Co_{0.4-x}Mg_xO_4$ phase.[22] The phase decomposition is closely associated with the loss of oxygen in the ceramics during sintering. Our results for the decomposition are in good agreement with those reported by previous workers.[2,23,24] They investigated the dependence of oxygen release on the temperature of the decomposition. As an example, Csete de Györgyfalva and Reaney[24] reported the decomposition in $NiMn_2O_4$ above 907 °C.

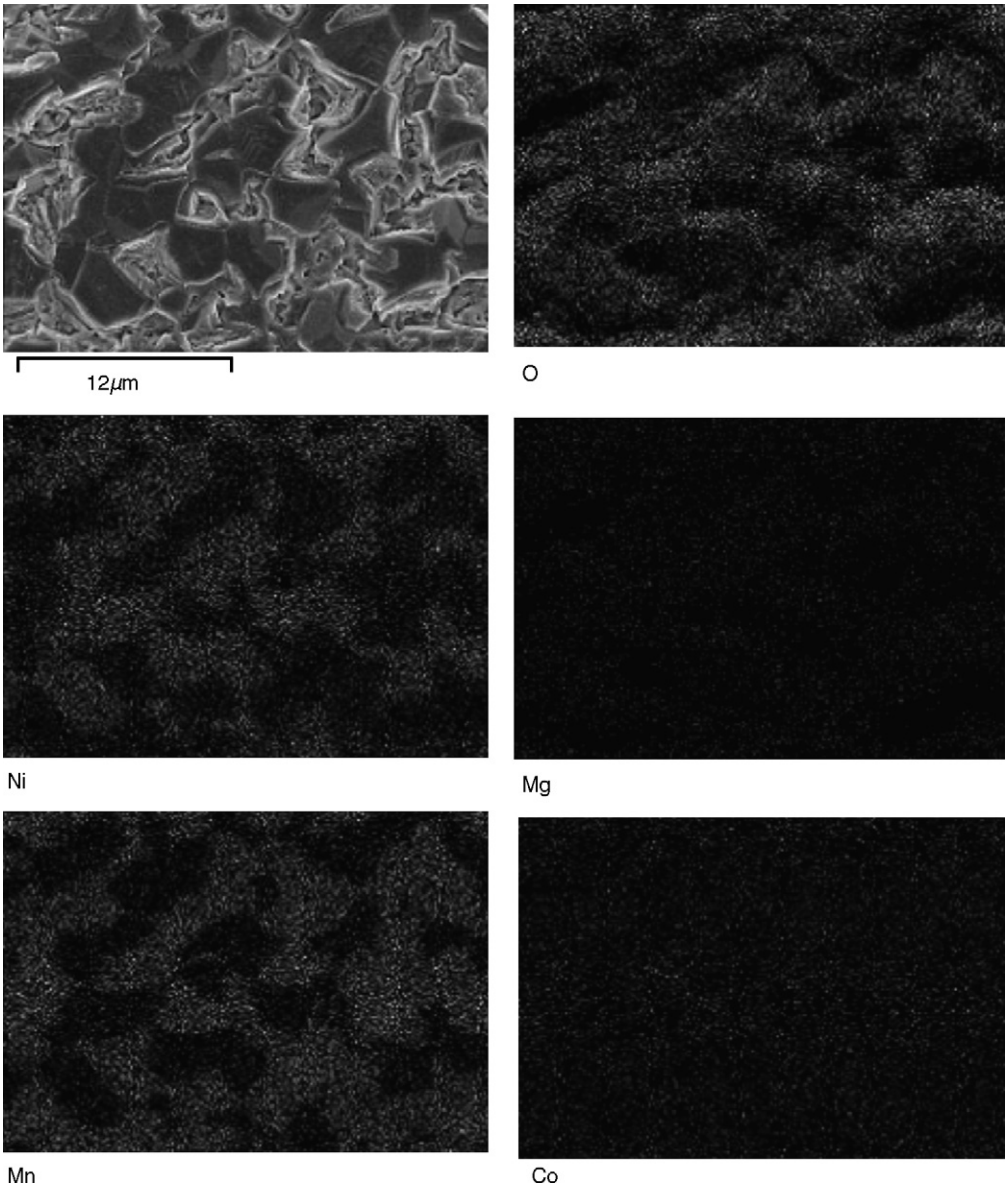

Fig. 5. SEI and maps of elements Mn, Ni, Co, Mg, and O for $Mn_{1.4}Ni_{1.2}Co_{0.2}Mg_{0.2}O_4$ sample sintered at 1260 °C.

In addition, the substituted Mg did not affect the crystalline structure and formed a solid solution with the two separated phases. The peaks corresponding to the Mn- and Ni-rich phases in the $Mn_{1.4}Ni_{1.2}Co_{0.2}Mg_{0.2}O_4$ sample slightly shifted towards higher angles with respect to the $Mn_{1.4}Ni_{1.2}Co_{0.4}O_4$ sample, indicating that the lattice parameter slightly decreases with an increase in Mg content. It is believed that the substituted Mg is present on substitutional sites in the cubic spinel lattice to form substitutional solid solutions. The ionic crystal radii of Co^{2+} and Mg^{2+} are 0.74 and 0.72 Å, respectively.[25] The lattice parameters of the Mn- and Ni-rich phases in the $Mn_{1.4}Ni_{1.2}Co_{0.4-x}Mg_xO_4$ samples are given in Table 1. It was also found that the intensity of the Ni-rich phase present in $Mn_{1.4}Ni_{1.2}Co_{0.2}Mg_{0.2}O_4$ sample is much lower than that in Mg-free $Mn_{1.4}Ni_{1.2}Co_{0.4}O_4$ sample, indicating that the substituted Mg suppressed the decomposition.

In order to conduct more detailed study of the decomposition of cubic spinel phase, green compacts were heated at lower temperatures (<1260 °C) for 3 h in air. It was found that the degree of the decomposition decreased with a decrease in the firing temperature. For example, the XRD patterns of the $Mn_{1.4}Ni_{1.2}Co_{0.4}O_4$ and $Mn_{1.4}Ni_{1.2}Co_{0.2}Mg_{0.2}O_4$ samples sintered at 950 °C are shown in Fig. 4(a and b), respectively. A very small amount of Ni-rich phase was observed, indicating that the low sintering temperature and the substituted Mg suppressed the decomposition.

We obtained SEI and several elemental maps from the $Mn_{1.4}Ni_{1.2}Co_{0.4-x}Mg_xO_4$ $(0 \le x \le 0.25)$ samples sintered at 1260 and 950 °C in order to confirm the phase decomposition. SEI and maps of elements Mn, Ni, Co, Mg, and O for one of the samples, $Mn_{1.4}Ni_{1.2}Co_{0.2}Mg_{0.2}O_4$, sintered at 1260 °C are shown in Fig. 5. In the sample, Mg and Co distributions were

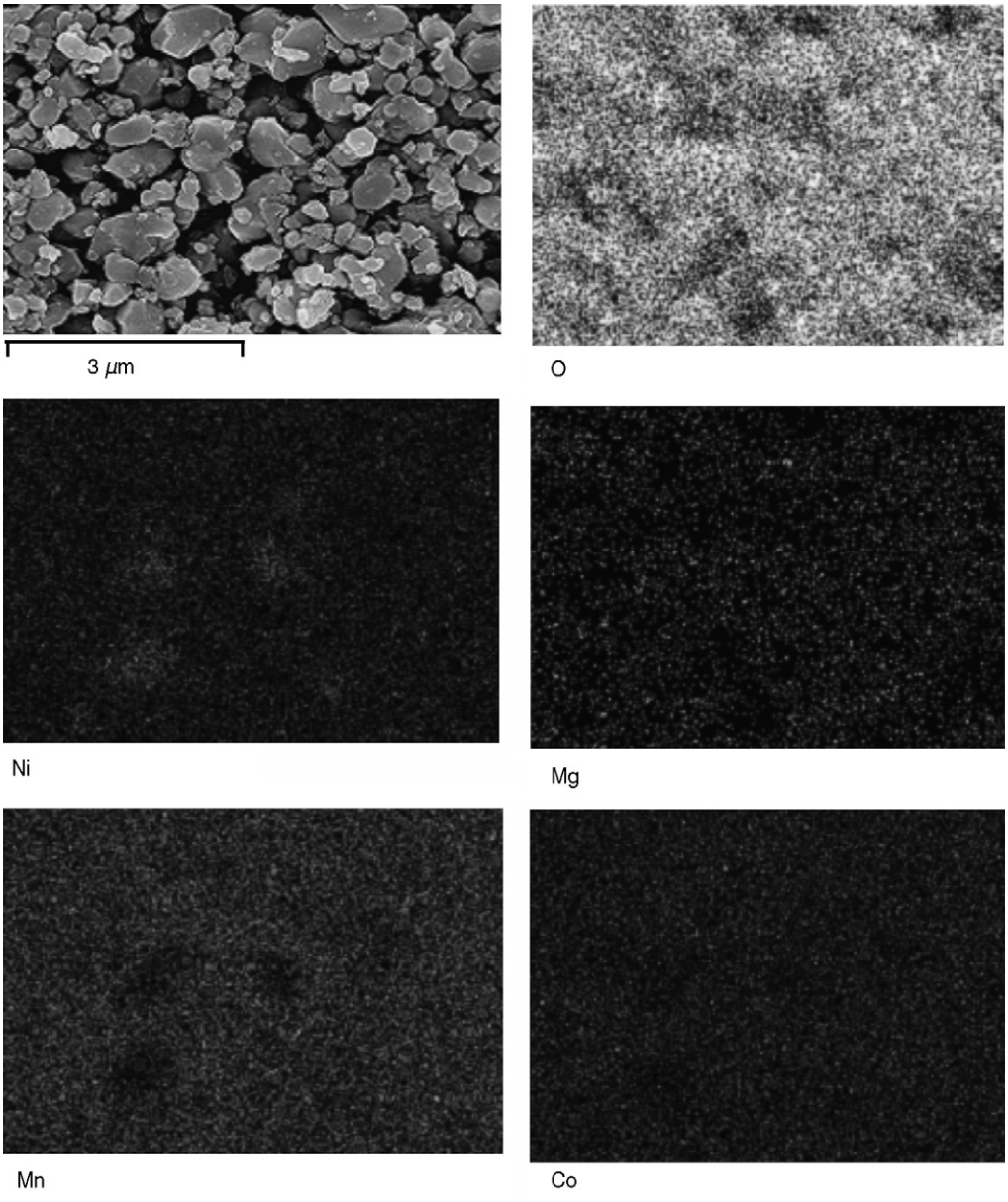

Fig. 6. SEI and maps of elements Mn, Ni, Co, Mg, and O for $Mn_{1.4}Ni_{1.2}Co_{0.2}Mg_{0.2}O_4$ sample sintered at 950 °C.

relatively homogeneous, while Ni, Mn, and O distributions were heterogeneous, regardless of innergrain and grain boundary. It is seen that the two decomposed Mn- and Ni-rich phases in the ceramics are present and some of the grains are oxygen deficient. These results strongly support the fact that the Ni-rich phase is decomposed in $Mn_{1.4}Ni_{1.2}Co_{0.4-x}Mg_xO_4$ solid solutions and the decomposition is closely associated with the loss of oxygen in the ceramics. In addition, we confirmed that the degree of the decomposition for the $Mn_{1.4}Ni_{1.2}Co_{0.4-x}Mg_xO_4$ ($0 \le x \le 0.25$) samples sintered at 950 °C was much lower than that at 1260 °C. As an example, SEI and elemental maps of the $Mn_{1.4}Ni_{1.2}Co_{0.2}Mg_{0.2}O_4$ sample sintered at 950 °C are shown in Fig. 6. The sintering temperature was insufficient to cause significant atomic diffusion for solid-state sintering (Fig. 7).

A plot of $\log \rho$ against the reciprocal of the absolute temperature ($1/T$) for the $Mn_{1.4}Ni_{1.2}Co_{0.4-x}Mg_xO_4$ ($0 \le x \le 0.25$) NTC thermistors is shown in Fig. 8. This figure reveals a nearly linear dependence of $\log \rho$ versus $1/T$ in the range of temperature measured, indicating semiconducting NTC thermistor characteristics. The slope of the $\log \rho$ versus $1/T$ curve is taken generally as a measure of the activation energy of conductivity. Also, the sensitivity index, the $B_{25/85}$ constant, is calculated from this figure. The $B_{25/85}$ constant is one of the most important characteristics of technical interest for NTC thermistors.

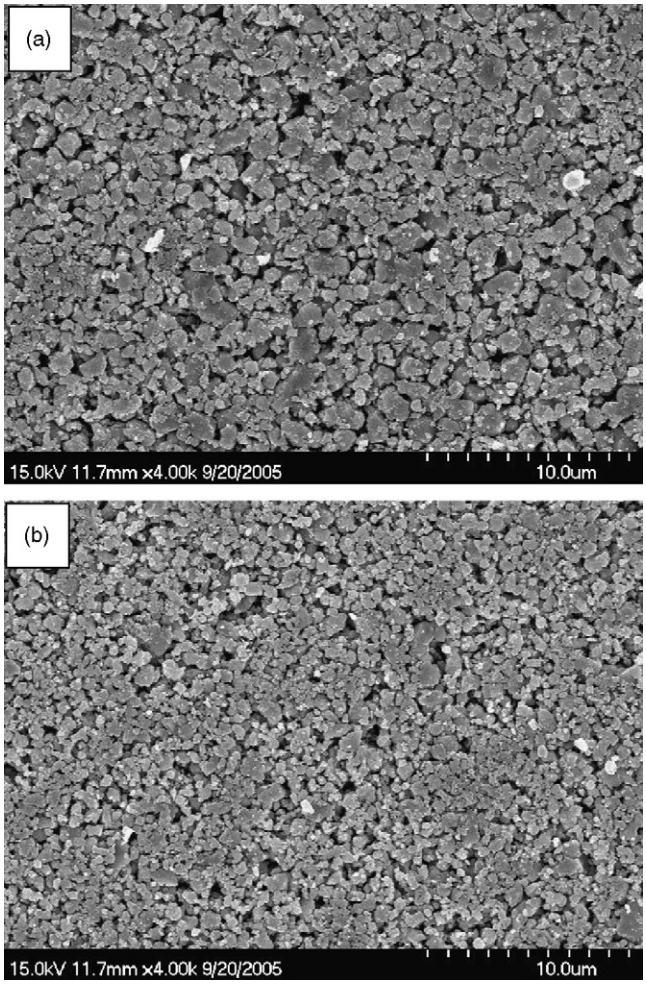

Fig. 7. SEM images obtained from the surface of: (a) $Mn_{1.4}Ni_{1.2}Co_{0.4}O_4$ and (b) $Mn_{1.4}Ni_{1.2}Co_{0.2}Mg_{0.2}O_4$ samples sintered at 950 °C.

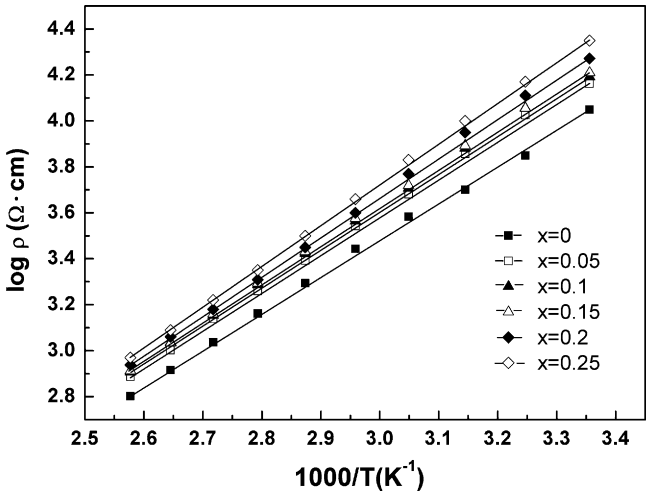

Fig. 8. A plot of $\log \rho$ against the reciprocal of the absolute temperature ($1/T$) for the $Mn_{1.4}Ni_{1.2}Co_{0.4-x}Mg_xO_4$ ($0 \le x \le 0.25$) NTC thermistors.

The calculated activation energy and $B_{25/85}$ constant of the $Mn_{1.4}Ni_{1.2}Co_{0.4-x}Mg_xO_4$ ($0 \le x \le 0.25$) NTC thermistors are listed in Table 2, together with the resistivity at 25 and 85 °C. The values of ρ_{25}, $B_{25/85}$ constant, and activation energy of the NTC thermistors with different compositions are 11,185–20,016 Ω cm, 3635–4032 K, and 0.313–0.348 eV, respectively. This indicates that the electrical properties of the NTC thermistors can be controlled by changing the composition. We found that, as the amount of MgO dopants increased, the resistivity increased. This can be explained as follows: (1) as discussed previously, both the grain size and density decreased with an increase in Mg content, resulting a decrease in the time between electron scattering events of charge carriers and thus increasing the resistivity. (2) As the amount of MgO in the thermistors increases, that of Co_3O_4 decreases, leading to a decrease in Co^{2+}/Co^{3+} ions on octahedral sites. In order to preserve the overall electrical neutrality of the material, some of the Mn^{4+} on octahedral sites change its valency to Mn^{3+}. This gives rise to a decrease in the amount of Mn^{3+}/Mn^{4+} ions on octahedral sites, which are responsible for hopping and conductivity,[26–30] resulting in an increase in the resistivity. It is also clear that the $B_{25/85}$ constant progressively increased with increasing Mg content, indicating an improvement in the thermistor sensitivity. For practical applications, a more higher value of the $B_{25/85}$ constant is desirable because its resistivity is more sensitive to variation of temperature, providing more accurate and smaller variation in temperature measurement. In addition, the activation energy of the thermistors increased with increasing Mg content. The activation energy is the energy for the hopping of electrons between the Mn^{3+} and Mn^{4+} ions on octahedral sites.[2–6,26–30]

On the basis of the above results, the values of measured electrical properties satisfy the requirements for being used as industrial NTC thermistors. Generally, the values of the $B_{25/85}$ constant and activation energy of the thermistors are 2000–7000 K and 0.1–1.5 eV, respectively.[31] The values of the resistivity and the $B_{25/85}$ constant are adjustable to desired values, dependent

Table 2
Resistivity at 25 and 85 °C, $B_{25/85}$ constant, and activation energy of the prepared $Mn_{1.4}Ni_{1.2}Co_{0.4-x}Mg_xO_4$ ($0 \le x \le 0.25$) NTC thermistors

Sample	Resistivity at 25 °C (Ω cm)	Resistivity at 85 °C (Ω cm)	$B_{25/85}$ constant (K)	Activation energy (eV)
$Mn_{1.4}Ni_{1.2}Co_{0.4}O_4$	11185	1450	3635	0.313
$Mn_{1.4}Ni_{1.2}Co_{0.35}Mg_{0.05}O_4$	14523	1817	3697	0.318
$Mn_{1.4}Ni_{1.2}Co_{0.3}Mg_{0.1}O_4$	15545	1935	3707	0.319
$Mn_{1.4}Ni_{1.2}Co_{0.25}Mg_{0.15}O_4$	16229	1967	3754	0.324
$Mn_{1.4}Ni_{1.2}Co_{0.2}Mg_{0.2}O_4$	18701	1991	3986	0.343
$Mn_{1.4}Ni_{1.2}Co_{0.15}Mg_{0.25}O_4$	20016	2077	4032	0.348

on the composition. It is thus concluded that the partial substitution of Mg for Co in $Mn_{1.4}Ni_{1.2}Co_{0.4}O_4$ is desirable for a wide range of practical applications of the NTC thermistors.

4. Conclusions

The sintered $Mn_{1.4}Ni_{1.2}Co_{0.4-x}Mg_xO_4$ ($0 \le x \le 0.25$) bodies were composed of the Mn- and Ni-rich phases with the cubic spinel structure, indicating a separation of Ni-rich phase in a $Mn_{1.4}Ni_{1.2}Co_{0.4-x}Mg_xO_4$ solid solution. The phase decomposition was likely to occur due to the loss of oxygen in the ceramics during sintering. The substituted Mg did not affect the crystalline structure and formed a $Mn_{1.4}Ni_{1.2}Co_{0.4-x}Mg_xO_4$ solid solution with the two decomposed phases. The grain size and density decreased with an increase in Mg content. The values of ρ_{25}, $B_{25/85}$ constant, and activation energy of the NTC thermistors were 11,185–20,016 Ω cm, 3635–4032 K, and 0.313–0.348 eV, respectively. In particular, the substituted Mg led to an increase in both the resistivity and the sensitivity index, the $B_{25/85}$ constant. It is concluded that the Mg substituted $Mn_{1.4}Ni_{1.2}Co_{0.4-x}Mg_xO_4$ ceramics are useful for industrial applications as NTC thermistors over a wide temperature range.

Acknowledgement

This work was supported by Small and Medium Business Administration in Korea.

References

1. Macklen, E. D., *Thermistors*. Electrochemical Publications Ltd., Ayr, Scotland, 1979.
2. Macklen, E. D., Electric conductivity and cation distribution in nickel manganite. *J. Phys. Chem. Solids*, 1986, **47**, 1073–1079.
3. Erickson, D. S. and Mason, T. O., Nonstoichiometry, cation distribution, and electrical properties in Fe_3O_4–$CoFe_2O_4$ at high temperature. *J. Solid State Chem.*, 1985, **59**, 42–53.
4. Feltz, A., Töpfer, J. and Schirrmeister, F., Conductivity data and preparation routes for $NiMn_2O_4$ thermistor ceramics. *J. Eur. Ceram. Soc.*, 1992, **9**, 187–191.
5. Dorris, S. E. and Mason, T. O., Electrical properties and cation valencies in Mn_3O_4. *J. Am. Ceram. Soc.*, 1988, **71**, 379–385.
6. Suzuki, M., *J. Phys. Chem. Solids*, 1980, **41**, 1253.
7. Larson, E. G., Arnott, R. J. and Wickham, D. G., Preparation, semiconduction and low-temperature magnetization of the system $Ni_{1-x}Mn_{2+x}O_4$. *J. Phys. Chem. Solids*, 1962, **23**, 1771–1781.
8. Golestani-Fard, F., Azimi, S. and Mackenzie, K. J. D., Oxygen evolution during the formation and sintering of nickel-manganese oxide spinels for thermistor applications. *J. Mater. Sci.*, 1987, **22**, 2847–2851.
9. Brabers, V. A. M., Setten, F. M. V. and Knapen, P. S. A., X-ray photoelectron spectroscopy study of the cation valencies in $NiMn_2O_4$. *J. Solid State Chem.*, 1981, **49**, 93–98.
10. Lavenuta, G., Negative temperature coefficient thermistors. *Sensors*, 1997, **14**, 46–55.
11. Mrooz, O., Kovalski, A., Pogorzelska, J., Shpotyuk, O., Vakiv, M., Butkiewicz, B. and Maciak, J., Thermoelectrical degradation processes in NTC thermistors for in-rush current protection of electronic circuits. *Microelectron. Reliability*, 2001, **41**, 773–777.
12. Fagan, J. G. and Amarkoon, V. R. W., Reliability and reproducibility of ceramic sensors: part I, NTC thermistors. *Am. Ceram. Soc. Bull.*, 1993, **72**, 70–79.
13. Sarkar, S. K., Sharma, M. L., Bhaskar, H. L. and Nagpal, K. C., Preparation, temperature and composition dependence of some physical and electrical properties of mixtures within the NiO–Mn_3O_4 system. *J. Mater. Sci.*, 1984, **19**, 545–551.
14. Larson, E. G., Arnott, R. J. and Wickham, D. G., Preparation, semiconduction and low-temperature magnetization of the system $Ni_{1-x}Mn_{2+x}O_4$. *J. Phys. Chem. Solids*, 1962, **23**, 1771–1781.
15. Fu, S. L. and Ho, I. C., The NTCR effect of V_2O_5-doped $(Ba_{0.8}Sr_{0.2})(Ti_{0.9}Zr_{0.1})O_3$ ceramics. *J. Mater. Sci. Lett.*, 1989, **8**(9), 999–1000.
16. Kshirsagar, S. T., Electrical and crystallographic studies of the system $Cu_xNi_{1-x}Mn_2O_4$. *J. Phys. Soc. Jpn.*, 1969, **27**, 1164–1170.
17. Metz, R., Caffin, J. P., Legros, R. and Rousset, A., The preparation, characterization and electrical properties of copper manganite spinels, $Cu_xMn_{3-x}O_4$, $0 \le x \le 1$. *J. Mater. Sci.*, 1989, **24**, 83–87.
18. Torikai, N., Meguro, T., Sasamoto, T., Nakayama, H., Yokoyama, T. and Abe, Y., Preparation of fine particles of spinel-type Mn–Co–Ni oxide by freeze-drying. *J. Chem. Soc. Jpn.*, 1984, 785–790.
19. Guillemet-Fritsch, S., Salmi, J., Sarrias, J., Rousset, A., Schuurman, S. and Lannoo, A., Mechanical properties of nickel manganites-based ceramics used as negative temperature coefficient thermistors (NTC). *Mater. Res. Bull.*, 2004, **39**, 1957–1965.
20. Gillot, B., Guendouzi, M. E., Kharroubi, M., Tailhades, P., Metz, R. and Rousset, A., Phase transformation-related kinetic in the oxidation of a manganese mixed oxide with a spinel structure. *Mater. Chem. Phys.*, 1989, **24**, 199–208.
21. Bennison, S. J. and Harmer, M. P., Grain-growth kinetics for alumina in the absence of a liquid phase. *J. Am. Ceram. Soc.*, 1985, **68**, C22–C24.
22. Meguro, T., Sasamoto, T., Yokoyama, T., Yamada, S., Abe, Y. and Torikai, N., Crystal structure change thermistor of Mn–Co–Ni oxides in firing process. *J. Jpn. Ceram. Soc.*, 1987, **95**, 336–340.
23. Jung, J., Töpfer, J., Mürbe, J. and Feltz, A., Microstructure and phase development in $NiMn_2O_4$ spinel ceramics during isothermal sintering. *J. Eur. Ceram. Soc.*, 1990, **6**, 351–359.
24. Csete de Györgyfalva, G. D. C. and Reaney, I. M., Decomposition of $NiMn_2O_4$ spinel: an NTC thermistor material. *J. Eur. Ceram. Soc.*, 2001, **21**, 2145–2148.
25. Kingery, W. D., Bowen, H. K. and Uhlmann, D. R., *Introduction to Ceramics*. John Wiley & Sons Inc., New York, 1976, p. 58.

26. Legros, R., Metz, R. and Rousset, A., Structural properties of nickel manganite $Ni_xMn_{3-x}O_4$ with $0.5 \leq x \leq 1$. *J. Mater. Sci.*, 1990, **25**, 4410–4414.
27. Battault, T., Legros, R. and Rousset, A., Structural and electrical properties of iron manganite spinels in relation with cationic distribution. *J. Eur. Ceram. Soc.*, 1995, **15**, 1141–1147.
28. Sarkar, S. K., Sharma, M. L. and Lahiri, S. K., Resistivity and *I–V* measurements of tetragonal Mn_3O_4 and dependence of nickel manganite on Mn_3O_4 content of NiO–Mn_3O_4 mixture. *J. Mater. Sci. Lett.*, 1987, **6**, 958–960.
29. Austin, I. G. and Mott, N. F., Polarons in crystalline and non-crystalline materials. *Adv. Phys.*, 1969, **18**, 41–102.
30. Jonker, G. H., Analysis of the semiconducting properties of cobalt ferrite. *J. Phys. Chem. Solids*, 1959, **9**, 165–175.
31. Martín de Vidales, J. L., García-Chain, P., Rojas, R. M., Vila, E. and García-Martínez, O., Preparation and characterization of spinel-type Mn–Ni–Co–O negative temperature coefficient ceramic thermistors. *J. Mater. Sci.*, 1998, **33**, 1491–1496.